Single-molecule optomechanics in 'pico-cavities'

Felix Benz[1], Mikolaj K. Schmidt[2], Alexander Dreismann[1], Rohit Chikkaraddy[1], Yao Zhang[2], Angela Demetriadou[2,3], Cloudy Carnegie[1], Hamid Ohadi[1], Bart de Nijs[1], Ruben Esteban[2], Javier Aizpurua[2,*], Jeremy J. Baumberg[1,*]

[1] NanoPhotonics Centre, Cavendish Laboratory, Department of Physics, JJ Thompson Ave, University of Cambridge, Cambridge, CB3 0HE, UK

[2] Materials Physics Center CSIC-UPV/EHU and Donostia International Physics Center DIPC, Paseo Manuel de Lardizabal, 20018 Donostia-San Sebastiàn, Spain

[3] Blackett Laboratory, Prince Consort Road, London, SW7 2AZ, UK

*Correspondence and requests for materials should be addressed to jjb12@cam.ac.uk, aizpurua@ehu.es

Trapping light with noble metal nanostructures overcomes the diffraction limit and can confine light to the nanometre scale (typically $\gtrsim$30 nm^3). Here we demonstrate individual atomic features inside the gap of a plasmonic nano-assembly localise light to volumes well below 1 nm^3 ('picocavities'), enabling optical experiments on the atomic scale. These atomic features are dynamically formed and disassembled by laser irradiation. While unstable at room temperature, picocavities can be stabilised at cryogenic temperatures, allowing single atomic cavities to be probed for many minutes. Unlike traditional optomechanical resonators, such extreme optical confinement yields million-fold-enhanced optomechanical coupling between the picocavity field and vibrations of individual molecular bonds. Picocavity formation probes the nanoscale, accessing sub-molecular dynamics and opens prospects for high precision sensors and single-photon strong-optomechanical coupling.

Coinage metal nanostructures support localised surface plasmons, which confine optical fields much tighter than their wavelength (*1*). This extreme enhancement enables vibrational spectroscopy within small volumes, even down to single molecules (*2*,*3*). For many years lateral resolution was believed to be ~10 nm (*4*), however recent experiments resolve the atomic structure of single molecules using tip-enhanced Raman spectroscopy (*3*) and directly sequence RNA strands (*5*). Atomistic simulations also suggest plasmonic confinement to atomic scales is possible (*6*). Here we show that light-activated mobilisation of surface atoms in a plasmonic hotspot triggers the formation of additional 'picocavities' bounded by a single gold atom. Their ultra-small light localisation alters which vibrational modes of trapped molecules are observed, due to strong optical field gradients that switch the Raman selection rules. The resulting cascaded ultra-strong plasmonic confinement pumps specific molecular bonds, thereby creating non-thermal vibrational populations, and forms a new type of optomechanical

resonator. Remarkably, cryogenic control of the plasmonic nanometric cavity allows for systematic and stable monitoring of the picocavity formation and disassembly. We thus show it is possible to resolve the dynamics of individual bonds within molecules. The existence, monitoring and selective control of these picocavities will be important not only in photochemistry and photophysics, but also as a new platform for optomechanics, coherent control and quantum information devices.

To produce stable robust picocavities we bypass complex scanning tip spectroscopies, instead using straightforward self-assembly to create 'nanoparticle-on-mirror' (NPoM) geometries (Fig.1A). Individual gold nanoparticles are spaced above a planar gold substrate by a nanometre-thick self-assembled monolayer of biphenyl-4-thiol (Fig.1B). Both the scattering and surface-enhanced Raman signals (SERS) from individual constructs are highly reproducible. All measurements are recorded at cryogenic temperatures, using a modified dark-field microscope and laser pumping at 633nm (see Materials and Methods). Low temperature time-series SERS spectra from a typical gold nanoparticle (Fig.1C) show vibrational modes that can be divided into two sets: a first set of vibrational modes is ever-present with constant intensity ('persistent lines'), while a second 'blinking' set of lines appears (arrows), disappears, and changes intensity over time.

Comparing the observed spectra with DFT simulations confirms that both types of lines originate from the biphenyl-4-thiol self-assembled monolayer. However, in the blinking set the relative intensities are altered and normally-Raman-inactive lines (infrared absorption lines) are mixed into the SERS spectrum. Which lines appear with which enhancement changes for each realisation of this fluctuating state, showing selective excitation of specific vibrations (additional spectra in (*7*), Fig.S13). By contrast, SERS intensities in the persistent set are unaffected by the appearance of blinking lines. As shown below, this suggests that blinking lines originate from a very small volume inside the plasmonic gap, containing only a single molecule. Such tight localisation yields extremely high field gradients, accounting for the observation of Raman-inactive infrared modes (*8*). Additional evidence implies these small hotspots are actually sub-nm^3 volumes that we term 'picocavities' consisting of only one gold atom. Full electromagnetic simulations (Fig.1D&E) show that picocavities locally boost the near-field intensity, leaving the rest of the plasmonic hotspot unaffected. The high field intensity within the extremely small <1nm^3 local hotspot (Fig.1D&E), dramatically enhances the SERS intensity of nearby molecules. We find that picocavities are spontaneously formed and destroyed under laser illumination, but can be stabilised.

Picocavities are atomic-scale sub-nanometric structures forming an extreme class of optical localisation that push electromagnetic coupling to the limit. To exploit and monitor their optical activity and to experimentally estimate the picocavity localization volume V_{loc}, we explore how they modify the

Raman scattering when exciting a molecular vibration. This process is dramatically amplified by the extreme confinement of the incident light in the plasmonic gap. As a result, the population n of excited vibrational states (at frequencies ω_m) is boosted above that provided by thermal excitations from the environment at temperature T, $n_{\mathrm{th}} = \left[\exp\left(\frac{\hbar\omega_m}{k_B T}\right) - 1\right]^{-1}$, by an additional contribution due to the optomechanical coupling of the plasmonic cavity with the molecular vibration (*9*). We first model the interaction of quantized plasmons with phonons in the classical limit of weak coupling g between the vibrations and cavity plasmons (with $g \ll \omega_m, \kappa$ for cavity decay rate κ), through the optomechanical Hamiltonian described in (*7*,*9*). This gives

$$n = \frac{\Gamma_{\mathrm{opt}}\, n_{\mathrm{rad}} + \Gamma_m n_{\mathrm{th}}}{\Gamma_{\mathrm{opt}} + \Gamma_m} \tag{1}$$

with volume-dependent optomechanical amplification rate $\Gamma_{\mathrm{opt}}(V_{\mathrm{loc}}) \propto g^2 I$ dependent on optomechanical coupling strength $g(V_{\mathrm{loc}})$ and laser power I, with phonon decay rate Γ_m (full expressions in (*7*), Section S1 and (*9*)). At T = 10K ($k_B T$ = 0.9meV), population n_{th} can be neglected because vibrational energies ($\hbar\omega_m = 124$meV for 1000cm^{-1}) greatly exceed thermal energies. Depending on the detuning of the laser from the cavity, Γ_{opt} can either be positive (damping the vibration) or negative (amplifying the vibration). For high enough intensities or strong enough coupling, amplification (Γ_{opt}) overcomes phonon decay (Γ_m) creating a non-thermal phonon population (dominating when $\Gamma_{\mathrm{opt}}\, n_{\mathrm{rad}} \gg \Gamma_m n_{\mathrm{th}}$). Experimentally measuring this vibrational state population at increasing laser power allows evaluation of the Raman localization volume V_{loc} (*7*).

In the regime of vibrational pumping, n can be quantified by simultaneously recording both the Stokes and anti-Stokes parts of the SERS spectrum and evaluating their ratio for each mode (*10*, *11*). The plasmon contribution to the population (arising from the quantum back-action mechanism) follows $n_{\mathrm{rad}} = [-4\omega_m\,(\omega_c - \omega_l)\,\mathcal{L}_-]^{-1}$ where $\mathcal{L}_\pm = [(\omega_c - \omega_l \pm \omega_m)^2 + (\kappa/2)^2]^{-1}$ is a Lorentzian profile of the field enhancement supported by the cavity resonance at frequency ω_c, illuminated by the laser with frequency ω_l. The ratio of anti-Stokes to Stokes scattering is then

$$\frac{S(\omega_{\mathrm{aS}})}{S(\omega_{\mathrm{S}})} \approx \left[\frac{\omega_l + \omega_m}{\omega_l - \omega_m}\right]^4 \frac{\mathcal{L}_-}{\mathcal{L}_+} \frac{n}{1+n}. \tag{2}$$

While the above analytic formalism is correct for coupling coefficients $g \ll \kappa$, in the conditions here corrections are needed from full numerical solution of the underlying optomechanical Hamiltonian (Eqs.S1&S2 in (*7*)) to properly extract estimates of the localization volume.

Crucially, low-temperature SERS shows that prominent anti-Stokes SERS lines blue-shifted from the laser (Fig.2A) appear always and only when the additional fluctuating Stokes lines are present. Time-

series SERS spectra (Fig.2B) show that none of the constant Stokes lines are seen in the anti-Stokes spectra (dashed lines), reflecting the low excited state population at 10K for most molecules within the NPoM gap but outside the picocavity. Taking the measured aS:S ratio, we use Eq. (2) in the thermal limit (setting $n = n_{\mathrm{th}}$) to extract for each vibrational mode an effective temperature (marked on Fig.2A), exceeding the sample temperature a hundredfold (up to 2000K for certain lines). These effective temperatures are different for each line, and increase with increasing vibrational energy, clear proof that the vibrational populations are non-thermal and that the pumping contribution to the population cannot be ignored. Plasmons do not directly heat the molecules, as shown by the absence of characteristic anti-Stokes background signals, previously shown to track the temperature of metallic nanostructures (*12*), and showing that the gold remains cold throughout, as expected for these sub-100μW optical powers.

In such time-series SERS scans, whenever the picocavity regime appears, spectral wandering of the vibrational energies of 0.1-1cm^{-1}s^{-1} is seen (Fig.2B), which is a typical signature of single-molecule SERS (*13*,*14*). This provides additional confirmation that the blinking lines come from a very small sub-region of the NPoM gap containing individual molecules. Further proof comes from observation of IR-active lines, which arise from the strong field gradients around the picocavity that alter the SERS selection rules (*3*,*8*) and necessarily require field localisation <0.5nm, consistent with picocavities in the nanogap. Theoretically, this effect can be reproduced by recalculating the SERS spectrum from the full Raman tensor (obtained by DFT) assuming only local illumination. Using a field localisation of 0.4nm, extracted from the picocavity field confinement lateral width (Fig.1D), the observed experimental spectra (Fig.2C,D bottom) can be modelled only when re-positioning the picocavity relative to the molecule (Fig.2C,D top, insets depict geometries used for each). To reproduce our experimental spectra, confinement on the order of a single gold atom is required (see Section S3 in (*7*)), giving direct proof for the atomic confinement of the optical field. In this regime, individual bonds within molecules can be accessed.

In order to use our Raman formalism to extract V_{loc}, we have to confirm that vibrational pumping dominates, for which a linear power dependence of the anti-Stokes to Stokes ratio is expected (*9*–*11*), as seen from Eq.(2) for small n. Previous investigations have found it challenging to stabilise nanostructures while measuring such power dependences. We achieve this by modifying our experiments to identify in real time whenever blinking lines appear, and then immediately cycling the laser power (Fig.3A shows typical data). We thus repeatedly record anti-Stokes:Stokes ratios for different 633nm laser powers. Extracting power series for several different lines (Fig.3B,C), recorded on different nanoparticles at different times, always gives a quadratic power dependence of the anti-Stokes signal and a linear power

dependence for the aS:S ratio (and hence phonon population), supporting the presence of vibrational pumping. However, the slope of these linear fits changes from mode to mode and also differs for different realisations on different nanoparticles. This suggests that the slope is a measure of picocavity geometry, which controls the different optomechanical coupling strengths of the molecular vibrations, since $g \propto 1/V_{\mathrm{loc}}$. From over 50 picocavities, we observe coupling strengths from g=5-40meV (Fig. 3D), reaching g/κ~0.2. From Eqs.(1),(S3) such high coupling strengths (compared to <1μeV for conventional optomechanical systems (*9*,*15*–*18*)) correspond to extremely small Raman localization volumes of <1nm^3 (see details in (*7*), Section S7). This extremely tight localisation agrees with electromagnetic simulations using atomic scale features in the gap region, also giving lateral localisations ≃0.23nm (FWHM of intensity, Fig.1E), as well as with previous theory predicting atom-scale confinement of optical fields (*6*,*19*). This optical confinement explains atomic resolution in tip-based experiments (*3*,*5*), and approaches the quantum limit derived previously (*4*), $V \simeq R d_{QR}^2$ however now with radius of curvature R set by the size of single atoms $R \sim 0.15$nm and tunnelling lengthscale $d_{QR} \sim 0.4$nm giving $V_{\min} \sim 10^{-2}$ nm^3. We highlight the strongly inhomogeneous distribution of picocavity field within the plasmonic gap, resulting in a complex relationship between the Raman localization volume and standard quantum optical definitions of mode volume (see (*7*), Section S5).

To account for both formation and disassembly of picocavities at cryogenic temperatures requires atomic surface reconstructions facilitated by irradiation. To demonstrate the dependence on laser power we immediately switch off the laser once the formation of a picocavity is detected. After a delay time varied between 3-30s the laser is switched on again (Fig.4A), allowing us to examine whether the atomic configuration relaxes in the dark. In all cases we find that the SERS spectra reappear with exactly the same strength as before the laser is switched off (see also Fig.S14 in (*7*)). This further proves that the additional strong Stokes and anti-Stokes SERS lines originate from a robust formation of these picocavities and not due to heating of the molecules - for a process involving heating one instead expects the system to cool back down once the laser is switched off.

Even when (instead of switching it off) the laser power is reduced, the lifetime of these picocavities is greatly extended (Fig.4B), thus allowing continuous monitoring. A picocavity is easily stabilised for more than 10min by reducing the laser power tenfold after cavity formation is observed. After 10min at the lower laser power the power is increased stepwise, and disassembly is observed at a laser power density of 100μW/μm^2. Both formation and disassembly of the picocavity are abrupt (sub-second), while fluctuations of the vibrational energies are found to increase as the laser power increases

(so the fluctuation of the molecular vibrational energies is possibly driven by Au atom movement, see Fig.4B and Fig.S12 in (*7*)).

Laser illumination not only destabilises the picocavity atomic configurations but is also crucial in their formation. To demonstrate this, we record several time-series SERS scans for different laser powers and extract the occurrence frequency of picocavity formation. We find a clear Arrhenius-type behaviour with critical laser power density $P_c = 256 \pm 15 \mu W/\mu m^2$, corresponding to an energy of 0.8eV (see Section S9 in (*7*)). This energy is comparable to previously reported activation energies for gold adatom surface diffusion of 0.9eV (*20*). Repeating the experiments using silver instead of gold gives a higher critical power density of $P_c = 388 \pm 48\ \mu W/\mu m^2$ but otherwise similar behaviour. Our observations are unable yet to identify whether this critical P_c corresponds to a characteristic thermal hopping barrier, or to optical forces arising from the extreme field gradients around single atom protrusions. However, we note that formation of a picocavity can be facilitated by the stability of gold-thiol 'staples': two thiols cooperatively pull a gold atom into an elevated position forming a bridge-like arrangement (see (*21*) and references therein). Our findings are also in line with observations that SERS blinking has both a thermal-activated and a light-activated component (*22*). Picocavities only show up in near-field-sensitive measurements such as SERS, while no changes are seen in far-field scattering that depend only on the properties of the larger hosting nanocavity. Our findings suggest picocavities are omnipresent in SERS and TERS measurements on nanoscale plasmonic hotspots such as colloidal aggregates, dimers, and NPoMs, and responsible for single-molecule and atomic resolution that has been obtained. The extreme optical confinement yields selective amplification of molecular vibrations of only a few bonds within the single molecule isolated by each picocavity, presumably depending on the exact mutual configuration of Au atom protrusion and bound thiol orientation. Optical field strengths of 0.3V/nm here may be further exploited.

We have shown the formation of stable atom-sized optical cavities termed 'picocavities' within plasmonic hotspots at cryogenic temperatures (which at room temperature are in constant dynamical creation and destruction). Picocavities form due to photon-assisted surface reconstruction of gold. Stabilising these picocavities while probing them takes plasmonic-molecule coupling to the extreme and opens widespread possibilities for studying and exploiting light-molecule coupling, for instance in molecular interactions, chemical reactions, superradiant emission, electron transfers, single-molecule electrochemistry, and advances the fundamental access of light to the building blocks of matter.

References and Notes

1. W. L. Barnes, A. Dereux, T. W. Ebbesen, Surface plasmon subwavelength optics. *Nature*. **424**, 824–830 (2003).

2. K. Kneipp *et al.*, Single Molecule Detection Using Surface-Enhanced Raman Scattering (SERS). *Phys. Rev. Lett.* **78**, 1667–1670 (1997).

3. R. Zhang *et al.*, Chemical mapping of a single molecule by plasmon-enhanced Raman scattering. *Nature*. **498**, 82–86 (2013).

4. K. J. Savage *et al.*, Revealing the quantum regime in tunnelling plasmonics. *Nature*. **491**, 574–577 (2012).

5. E. Bailo, V. Deckert, Tip-Enhanced Raman Spectroscopy of Single RNA Strands: Towards a Novel Direct-Sequencing Method. *Angew. Chem. Int. Ed.* **47**, 1658–1661 (2008).

6. M. Barbry *et al.*, Atomistic Near-Field Nanoplasmonics: Reaching Atomic-Scale Resolution in Nanooptics. *Nano Lett.* **15**, 3410–3419 (2015).

7. See Supplementary Materials on Science Online for details.

8. M. Moskovits, D. P. DiLella, K. J. Maynard, Surface Raman spectroscopy of a number of cyclic aromatic molecules adsorbed on silver: selection rules and molecular reorientation. *Langmuir*. **4**, 67–76 (1988).

9. M. K. Schmidt, R. Esteban, A. González-Tudela, G. Giedke, J. Aizpurua, Quantum Mechanical Description of Raman Scattering from Molecules in Plasmonic Cavities. *ACS Nano*. **10**, 6291–6298 (2016).

10. R. C. Maher, C. M. Galloway, E. C. L. Ru, L. F. Cohen, P. G. Etchegoin, Vibrational pumping in surface enhanced Raman scattering (SERS). *Chem. Soc. Rev.* **37**, 965–979 (2008).

11. D. R. Ward, D. A. Corley, J. M. Tour, D. Natelson, Vibrational and electronic heating in nanoscale junctions. *Nat. Nanotechnol.* **6**, 33–38 (2011).

12. J. T. Hugall, J. J. Baumberg, Demonstrating Photoluminescence from Au is Electronic Inelastic Light Scattering of a Plasmonic Metal: The Origin of SERS Backgrounds. *Nano Lett.* **15**, 2600–2604 (2015).

13. S. Nie, S. R. Emory, Probing Single Molecules and Single Nanoparticles by Surface-Enhanced Raman Scattering. *Science*. **275**, 1102–1106 (1997).

14. C. C. Neacsu, J. Dreyer, N. Behr, M. B. Raschke, Scanning-probe Raman spectroscopy with single-molecule sensitivity. *Phys. Rev. B*. **73**, 193406 (2006).

15. R. Esteban, T. V. Teperik, J. J. Greffet, Optical Patch Antennas for Single Photon Emission Using Surface Plasmon Resonances. *Phys. Rev. Lett.* **104**, 26802 (2010).

16. X. Zeng *et al.*, Metallo-dielectric hybrid antenna for high Purcell factor and radiation efficiency. *Opt. Express*. **22**, 14517 (2014).

17. M. Liu, T.-W. Lee, S. K. Gray, P. Guyot-Sionnest, M. Pelton, Excitation of Dark Plasmons in Metal Nanoparticles by a Localized Emitter. *Phys. Rev. Lett.* **102**, 107401 (2009).

18. X.-W. Chen, M. Agio, V. Sandoghdar, Metallodielectric Hybrid Antennas for Ultrastrong Enhancement of Spontaneous Emission. *Phys. Rev. Lett.* **108**, 233001 (2012).

19. X. Chen, J. E. Moore, M. Zekarias, L. Jensen, Atomistic electrodynamics simulations of bare and ligand-coated nanoparticles in the quantum size regime. *Nat. Commun.* **6**, 8921 (2015).

20. T.-S. Lin, Y.-W. Chung, Measurement of the activation energy for surface diffusion in gold by scanning tunneling microscopy. *Surf. Sci.* **207**, 539–546 (1989).

21. T. Bürgi, Properties of the gold–sulphur interface: from self-assembled monolayers to clusters. *Nanoscale*. **7**, 15553–15567 (2015).

22. S. R. Emory, R. A. Jensen, T. Wenda, M. Han, S. Nie, Re-examining the origins of spectral blinking in single-molecule and single-nanoparticle SERS. *Faraday Discuss*. **132**, 249–259 (2006).

23. M. Hegner, P. Wagner, G. Semenza, Ultralarge atomically flat template-stripped Au surfaces for scanning probe microscopy. *Surf. Sci.* **291**, 39–46 (1993).

24. P. Roelli, C. Galland, N. Piro, T. J. Kippenberg, Molecular cavity optomechanics as a theory of plasmon-enhanced Raman scattering. *Nat. Nanotechnol.* **11**, 164–169 (2016).

25. M. Aspelmeyer, T. J. Kippenberg, F. Marquardt, Cavity optomechanics. *Rev. Mod. Phys.* **86**, 1391–1452 (2014).

26. M. Hinreiner *et al.*, Influencing the conductance in biphenyl-like molecular junctions with THz radiation. *Phys. Status Solidi B*. **250**, 2408–2416 (2013).

27. F. Ho, W.-S. Tsay, J. Trout, R. M. Hochstrasser, Direct measurement of the vibrational relaxation of the 991 cm^{-1} mode of the benzene crystal. *Chem. Phys. Lett.* **83**, 5–9 (1981).

28. F. Benz *et al.*, SERS of Individual Nanoparticles on a Mirror: Size Does Matter, but so Does Shape. *J. Phys. Chem. Lett.* **7**, 2264–2269 (2016).

29. R. Esteban *et al.*, A classical treatment of optical tunneling in plasmonic gaps: extending the quantum corrected model to practical situations. Faraday Discuss. 178, 151–183 (2015).

30. A. F. Koenderink, On the use of Purcell factors for plasmon antennas. *Opt. Lett.* **35**, 4208 (2010).

31. C. Sauvan, J. P. Hugonin, I. S. Maksymov, P. Lalanne, Theory of the Spontaneous Optical Emission of Nanosize Photonic and Plasmon Resonators. *Phys. Rev. Lett.* **110**, 237401 (2013).

32. R. Esteban, J. Aizpurua, G. W. Bryant, Strong coupling of single emitters interacting with phononic infrared antennae. New J. Phys. 16, 13052 (2014).

33. H. T. Dung, L. Knöll, D.-G. Welsch, Three-dimensional quantization of the electromagnetic field in dispersive and absorbing inhomogeneous dielectrics. Phys. Rev. A. 57, 3931–3942 (1998).

34. P. T. Kristensen, S. Hughes, Modes and Mode Volumes of Leaky Optical Cavities and Plasmonic Nanoresonators. ACS Photonics. 1, 2–10 (2014).

35. A. Delga, J. Feist, J. Bravo-Abad, F. J. Garcia-Vidal, Quantum Emitters Near a Metal Nanoparticle: Strong Coupling and Quenching. Phys. Rev. Lett. 112, 253601 (2014).

We acknowledge financial support from EPSRC grants EP/G060649/1 and EP/L027151/1, and ERC grant LINASS 320503. MKS, YZ, AD, RE, and JA acknowledge financial support from Project FIS2013- 41184-P from MINECO and IT756-13 from the Basque Government consolidated groups. FB acknowledges support from the Winton Programme for the Physics of Sustainability. RC acknowledges support from the Dr. Manmohan Singh scholarship from St. John's College. CC thanks NPL for support. RE acknowledges support from the Fellows Gipuzkoa Program of the Gipuzkoako Foru Aldundia via FEDER funds of the European Union "Una manera de hacer Europa".

Source data can be found at DOI: 10.17863/CAM.1675

Supplementary material

Materials and Methods

Theoretical model of molecular optomechanics, Calculation of the coherent pumping parameter, Localised DFT simulations, Spectral response of the picocavity, Calculation of the mode volume from numerical calculations, Reference measurements on silicon, Estimation of the mode volume from the measured anti-Stokes/Stokes ratio, Silver nanoparticle-on-mirror experiments, Picocavity formation statistics, Spectral wandering, Additional experimental anti-Stokes spectra, Picocavity stability under laser illumination, Reference measurements of biphenyl-4-thiol powder, and Reference measurements at room temperature.

Figures S1 – S16

References 23-35

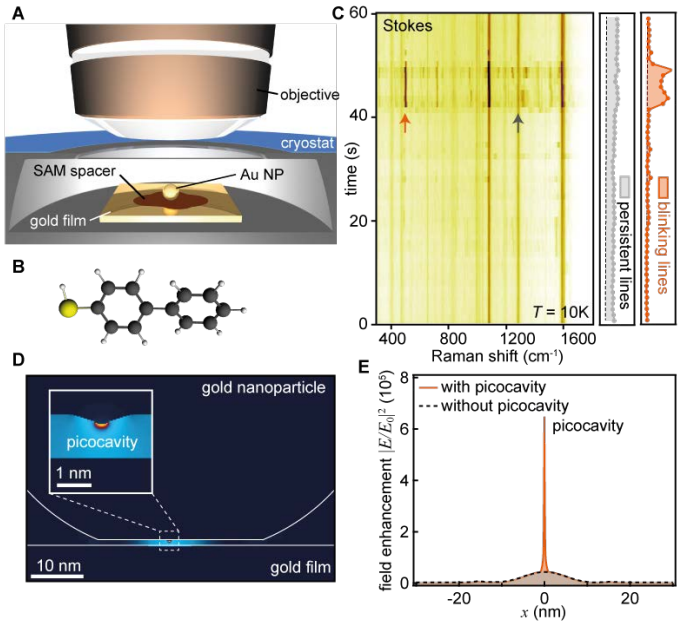

Figure 1 | Raman spectra from molecules in picocavity and near-field light distribution. (A) Schematic cooled nanoparticle-on-mirror (NPoM) geometry. (B) Biphenyl-4-thiol molecular monolayer. (C) SERS time series from a single 90nm NPoM with 60μW/μm^2 pump. (D-E) Simulations of facetted gold nanoparticle with(out) atomic protrusion at x=0 nm. (D) Near-field map, inset: enlarged view of picocavity, showing sub-nanometre localisation of optical field. (E) Near-field intensity across the gap.

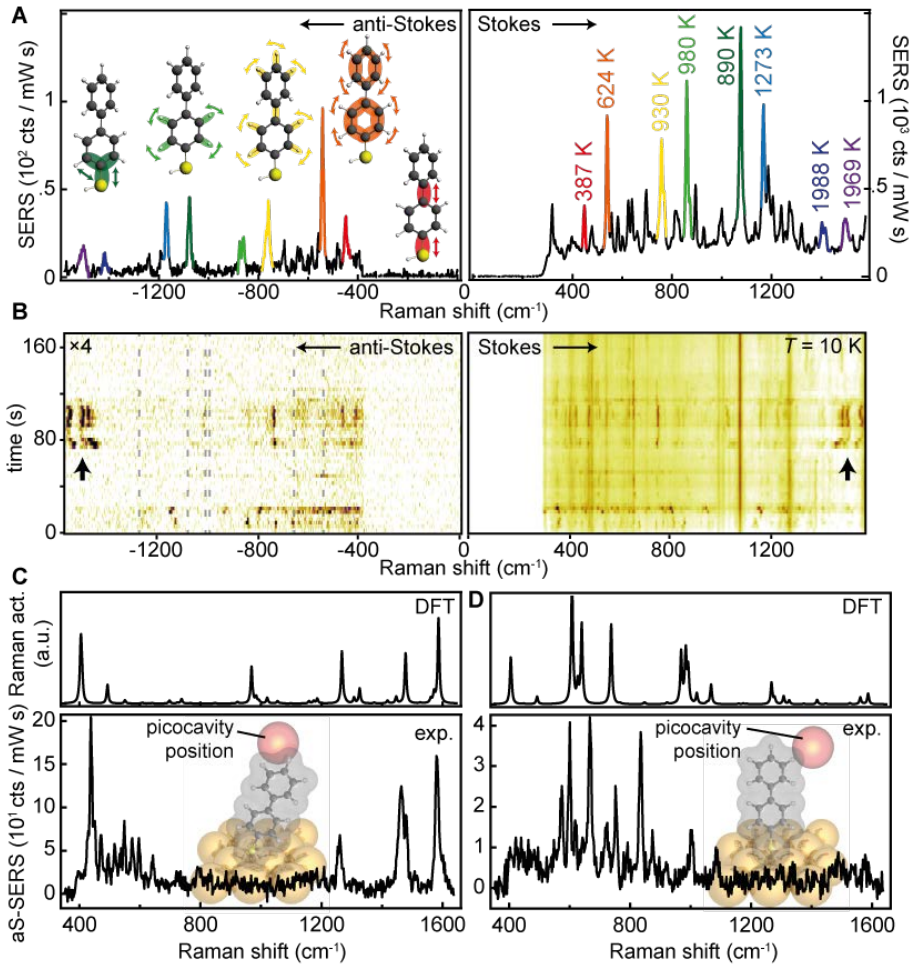

Figure 2 | Raman spectra reveal changes of SERS selection rules. (A) Anti-Stokes:Stokes spectra at a time when additional picocavity-induced lines are present. Colours correspond to same lines on Stokes and anti-Stokes sides, with vibrational eigenmodes and effective temperatures shown. (B) Time-series anti-Stokes and Stokes SERS. Dashed lines (aS) mark expected aS line positions corresponding to ever-present (persistent) S lines from the many molecules in the larger nanocavity. (C,D) Comparison of two experimental spectra (bottom) with DFT simulated spectra (top) under the assumption of atomic-scale field confinement (inset shows geometries, red sphere shows field localisation for simulations).

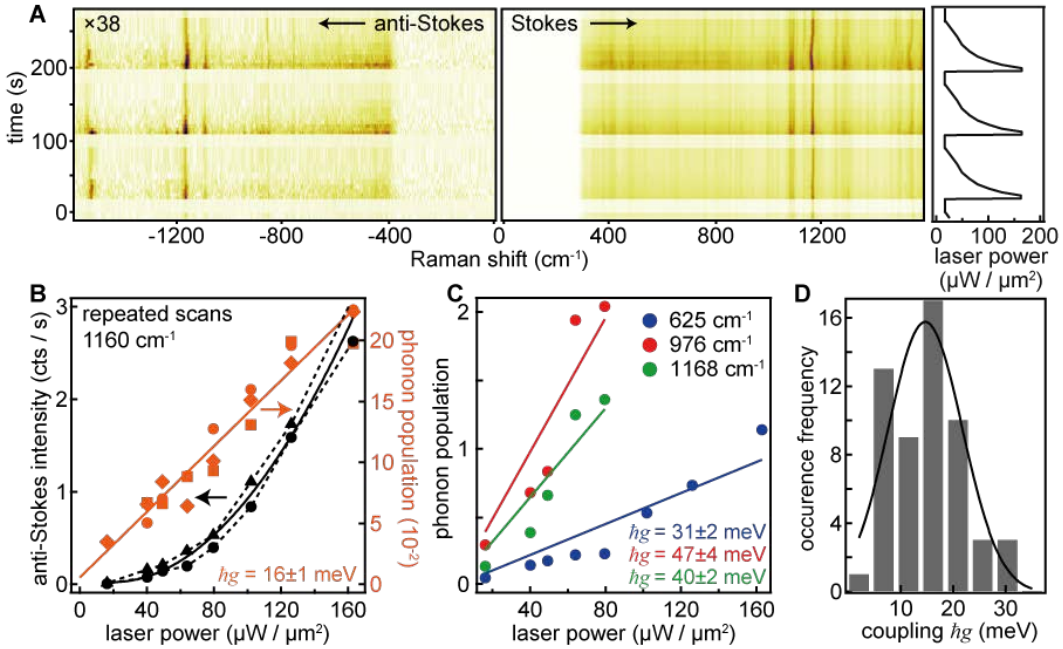

Figure 3 | Vibrational pumping of molecular vibrations in picocavities. (A) SERS time scan for varying laser power (shown on right). (B) Extracted laser power dependence of anti-Stokes intensity and phonon population, for different measurements on the same picocavity. (C) Power dependence of phonon population for different vibrational modes in the same picocavity. (D) Distribution of observed optomechanical coupling strengths g.

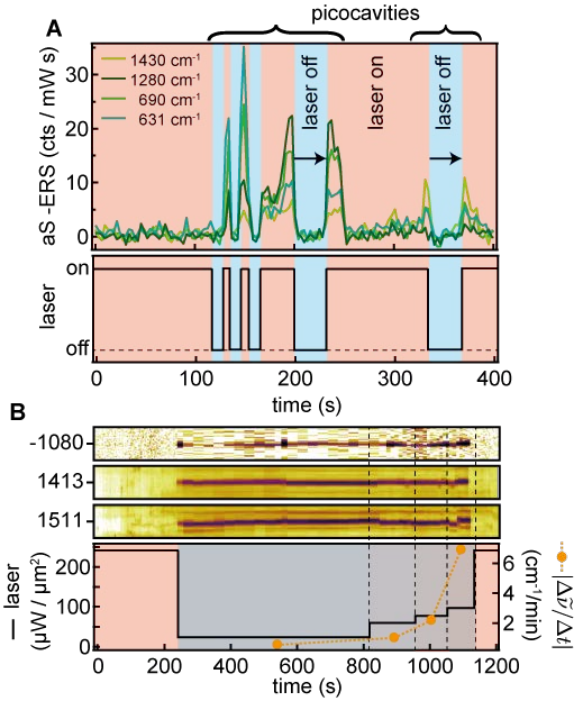

Figure 4 | Picocavity stability in the dark. (A) Anti-Stokes intensities as the laser (bottom) is switched on/off demonstrate the picocavity stability, which persists (arrows) without laser. (B) Picocavities are also stable at low laser powers. Anti-Stokes intensities as laser power is dropped ten-fold when picocavity formation is detected. After waiting 10min the power is stepwise increased. SERS intensities shown normalised by laser power. Simultaneously-measured rate of spectral wandering (orange) vs laser power shown on lower graph.